JOURNAL OF THE MECHANICAL BEHAVIOR OF BIOMEDICAL MATERIALS 20 (2013) 173–183

Available online at www.sciencedirect.com
SciVerse ScienceDirect
www.elsevier.com/locate/jmbbm

Research Paper

Chitosan membranes containing micro or nano-size bioactive glass particles: evolution of biomineralization followed by *in situ* dynamic mechanical analysis

Sofia G. Caridade[a,b], *Esther G. Merino*[a,b], *Natália M. Alves*[a,b], *Verónica de Zea Bermudez*[c], *Aldo R. Boccaccini*[d], *João F. Mano*[a,b,*]

[a]*3B's Research Group – Biomaterials, Biodegradables and Biomimetics, University of Minho, Headquarters of the European Institute of Excellence on Tissue Engineering and Regenerative Medicine, AvePark, 4806-909 Taipas, Guimarães, Portugal*
[b]*ICVS/3B's – PT Government Associate Laboratory, Braga/Guimarães, Portugal*
[c]*Department of Chemistry/CQ-VR, University of Trás-os-Montes e Alto Douro, 5001-801 Vila Real, Portugal*
[d]*Institute for Biomaterials, Department of Materials Science and Engineering, University of Erlangen-Nuremberg, Cauerstr. 6, 91058 Erlangen, Germany*

ARTICLE INFO

Article history:
Received 5 September 2012
Received in revised form
13 November 2012
Accepted 19 November 2012
Available online 20 December 2012

Keywords:
Nanocomposites
Bioactive glass
Dynamic mechanical analysis
Bioactivity
Bone regeneration

ABSTRACT

A new family of biodegradable polymer/bioactive glass (BG) composite materials has emerged based on the availability of nano-sized bioactive particles. Such novel biocomposites can have enhanced performance, in terms of mechanical properties and bioactivity, and they can be designed to be used in bone regeneration approaches.

In this work, membranes of chitosan (CTS) and chitosan with bioactive glass (BG) both micron and nano sized particles (CTS/μBG, CTS/nBG, respectively) were prepared by solvent casting. Microstructural and mechanical properties were evaluated in order to compare the effects of the incorporation of micro (μBG) and nano (nBG) particles in the chitosan matrix. *In vitro* bioactivity tests were performed to characterize the apatite layer that is formed on the surface of the material after being immersed in simulated body fluid (SBF). The biomineralization process on the biomaterials was also followed using non-conventional dynamic mechanical analysis (DMA), both online and offline. In such DMA experiments, the change in the storage modulus, E', and the loss factor, tan δ, were measured as a function of the immersion time in SBF. The results demonstrated that CTS/nBG membranes possess enhanced mechanical properties and higher bioactivity in comparison with the CTS/μBG membranes. Such results suggest the potential of nBG for the development of bioactive composites for bone regeneration applications.

*Corresponding author at: 3B's Research Group – Biomaterials, Biodegradables and Biomimetics, University of Minho, Headquarters of the European Institute of Excellence on Tissue Engineering and Regenerative Medicine, AvePark, 4806-909 Taipas, Guimarães, Portugal.
E-mail addresses: sofia.caridade@dep.uminho.pt (S.G. Caridade), egarciamerino@yahoo.es (E.G. Merino), nalves@dep.uminho.pt (N.M. Alves), vbermude@utad.pt (V.d.Z. Bermudez), Aldo.Boccaccini@ww.uni-erlangen.de (A.R. Boccaccini), jmano@dep.uminho.pt (J.F. Mano).

1751-6161/$ - see front matter © 2012 Elsevier Ltd. All rights reserved.
http://dx.doi.org/10.1016/j.jmbbm.2012.11.012

1. Introduction

Composite materials, based on polymer and bioactive ceramics and glasses, have gained enormous attention, in the past years, for a variety of biomedical applications. Several studies demonstrate that the combination of the properties of polymers and bioactive ceramics leads to optimal performance for applications in areas such as bone regeneration (Rezwan et al., 2006). The polymer's role is to serve as the matrix to support cell growth, which is based on convenient polymers properties such as biodegradability, biocompatibility and flexibility. On the other hand, the incorporation of inorganic particles such as hydroxyapatite or bioactive glass has the dual aim to improve the mechanical properties as well as to provide bioactivity to the device. For that reason, composites based on biodegradable polymers containing bioactive ceramics or glasses are effective in preserving the structural and biological functions of damaged hard tissues and they mimick more closely the natural system (Gloria et al., 2010; Luz and Mano, 2010) in comparison to polymers or ceramics taken separately. Different approaches have been proposed to provide osteoconductive properties in biomaterials intended for bone regeneration purposes (Alves et al., 2010a; Kim et al., 2005a; Oliveira et al., 2003). A simple way is to introduce bioactive inorganic particles or fibers into the polymeric matrix (Alves et al., 2010a; Boccaccini et al., 2010; Rezwan et al., 2006). Although the combination of such materials has been mainly reported by using conventional, micron-size, bioactive glass particles (Rezwan et al., 2006), some recent studies report the use of nano-sized bioactive glass (BG), as reviewed elsewhere (Boccaccini et al., 2010). Such novel composite materials appear to be relevant for use in bone defects/bone regeneration approaches since it is expected that they exhibit enhanced performance in terms of mechanical properties and bioactivity (Boccaccini et al., 2010; Swetha et al., 2010).

One important parameter that affects the mechanical properties of composite materials is the size of the inclusions because it influences the interactions between the filler particles and the polymer matrix. Nanoscale bioactive particles possess a higher specific surface area than the microscale ones forming a tighter interface with the polymer matrix in composites, and therefore a high performance in mechanical properties and processing can be expected (Hong et al., 2005; Juhasz et al., 2004). Moreover, the higher specific surface area of nanoparticles allows not only for a faster release of ions (higher bioreactivity) but also a higher protein adsorption ability, which results in enhanced bioactivity (Loher et al., 2006; Misra et al., 2008; Vollenweider et al., 2007). Additionally, the use of nanoparticles in a polymeric matrix mimics more closely the structure of natural bone, which contains nanoscale hydroxyapatite crystallites, being responsible for the high strength of bone, combined with the polymeric phase of collagen (Kay et al., 2002; Palin et al., 2005). Mimicking the nanofeatures of bone on the surface of a synthetic implant material also provides more active sites for osteoblast cell attachment and tissue growth (Kim et al., 2005b; Webster et al., 1999; Wheeler et al., 1998).

In this work, membranes of chitosan (CTS), chitosan micro-sized bioactive glass (CTS/μBG) and chitosan nano-sized bioactive glass (CTS/nBG) were prepared by solvent casting. The motivation was to compare the differences in the structural and mechanical properties as well as in bioactivity by using both micron and nano sized bioactive glass particles in the polymeric matrix. The bioactivity of composites has been typically followed, *in vitro*, by monitoring the formation of an apatite layer on the surface of the biomaterial after being immersed in SBF (Kokubo and Takadama, 2006); the characterization of such apatite layer is done at pre-determined time points after samples are soaked in the SBF solution. Information about the formation of this apatite layer, in real time, may provide relevant cues about the kinetics and mechanism of calcification; this could help in explaining the evolution of the properties of the biomaterial. It is worthwhile noticing that until now just few studies have followed the biomineralization process *in situ* (Cerruti et al., 2005; Eliaz et al., 2009; Leonor et al., 2003). Therefore, we propose here to investigate the formation of the apatite layer, in real time, over the bioactive composite surfaces upon immersion in SBF using *in situ* dynamic mechanical analysis (DMA). It is expected that such experiments are relevant to predict the evolution of the mechanical performance of bioactive medical devices upon implantation. Indeed DMA has been used previously extensively to characterize biomaterials (Mano, 2002). However, other mechanical techniques have been used to characterize soft biotissues and polymers, such as, nanoindentation (Ebenstein and Pruitt, 2004, 2006; Franke et al., 2007, 2011; Nayar et al., 2012; Strange and Oyen, 2012). To our knowledge, however, this is the first time that composites containing micron and nano sized bioactive glass nanoparticles are characterized and compared in terms of calcification using *in situ* DMA tests.

2. Materials and methods

2.1. Materials

Chitosan (medium molecular weight) was purchased from Sigma–Aldrich, Germany, and was purified prior to use. The degree of *N*-deacetylation (DD) was found to be 78.7% by the first derivative ultraviolet spectrophotometry, using both glucosamine (GluN) and *N*-acetylglucosamine (GluNAc) standards for calibration (da Silva et al., 2008). The molecular weight (M_v) was determined by viscometry in CH_3COOH 0.5 M/$NaCH_3COO$ 0.2 M, which was found to be 770 kDa according to the Mark–Houwing theory ($k=3.5\times10^{-4}$; $a=0.76$) (Terbojevich et al., 1996). Micro-sized bioactive glass particles of Bioglass® (45S5) composition (45 wt% SiO_2, 24.5 wt% CaO, 24.5 wt% Na_2O, 6 wt% P_2O_5) (Hench, 1998) with an average particle size of 5 μm was supplied by US Biomaterials Corp. (Florida, USA). Bioactive glass nanoparticles with chemical composition close to 45S5 Bioglass®: 46.08 wt% SiO_2–22.96 wt% Na_2O–27.18 wt% CaO–3.77 wt% P_2O_5 were prepared by flame spray synthesis (Madler et al., 2002) as described in detail by Brunner et al. (2006). The SBF was prepared by dissolving NaCl (ACS reagent, ≥99.0% purity), $NaHCO_3$ (ACS reagent, ≥99.7% purity), KCl (ACS reagent, ≥99.0% purity), $K_2HPO_4\cdot3H_2O$ (ReagentPlus®, ≥99.0% purity), $MgCl_2\cdot6H_2O$ (ACS reagent, ≥99.0% purity), $CaCl_2$ (ACS reagent, ≥96.0% purity) and Na_2SO_4 (ACS reagent, ≥99.0%

purity) in distilled water and buffered with Tris buffer (ACS reagent, ≥99.8% purity) and HCl (ACS reagent) to reach a pH value of 7.4. All chemicals for simulated body fluid (SBF) preparation were obtained from Sigma–Aldrich, Germany. All other reagents and solvents used were of reagent grade and were used without further purification.

2.2. Membranes preparation

Chitosan (CTS), chitosan/micro BG (CTS/μBG) and chitosan/nano BG (CTS/nBG) membranes were prepared by solvent casting. First, 1 wt% chitosan was dissolved in 1 wt% aqueous acetic acid (glacial, ACS reagent, ≥99.7% – Sigma Aldrich) and filtered to remove impurities. For the composite membranes, 30 wt% of BG particles were added to the polymer solution. This mixture was stirred for 2 h and then sonicated for 15 min. The solutions were cast in Petri dishes and left to dry at room temperature. After drying, CTS, CTS/μBG and CTS/nBG composite membranes were peeled off and neutralized in a 0.1 M NaOH (ACS reagent, ≥97.0%, pellets) solution for about 10 min, washed thoroughly with distilled water and dried again at room temperature. The thickness of the films was about 50 μm.

2.3. Bioactivity tests

For the *in vitro* bioactivity tests, an acellular simulated body fluid (SBF) (1.0x) was prepared, with ions concentration nearly equal to human blood plasma. The SBF composition and preparation were previously described by Kokubo and Takadama (2006). Sample membranes of $20 \times 15\ mm^2$ were cut from the original processed films. Three replicates for each sample were immersed in SBF for 1, 5 and 7 days at 37 °C. After being removed from SBF, the samples were gently rinsed with distilled water and dried at room temperature.

2.4. Physical characterization of materials

2.4.1. Transmission electron microscopy (TEM)

The nBG particles were analyzed prior to composite preparation by Transmission Electron Microscopy. TEM image of the nBG particles was recorded on a CM 30 ST (Philips, LaB6 cathode, operated at 300 kV, point resolution 4 Å).

2.4.2. Scanning electron microscopy (SEM)

The morphological analysis of the samples (after and before bioactivity test) was performed using Scanning Electron Microscope (SEM, Leica Cambridge S 360) at an accelerated voltage of 15 kV. Before being observed by SEM, the membranes were gold coated using a Hitachi coater at 6 mA.

2.4.3. Energy dispersive spectroscopy (EDS)

Samples were observed by a Leica Cambridge S360 Scanning Electron Microscope. The samples were fixed by mutual conductive adhesive tape on aluminum and covered with carbon using a sputter coater. After immersion in SBF the samples were again analyzed in order to visualize the appearance of a calcium-phosphate layer on their surfaces.

2.4.4. Thin-film X-ray diffraction (TF-XRD)

TF-XRD analyses on samples before and after 7 days of immersion in SBF were performed to characterize the crystalline/amorphous nature of the films and to identify any crystalline phases present after immersion in SBF. The membranes were analyzed recording the wide-angle X-ray scattering patterns in a Philips PW1710 reflection diffractometer (Almelo, The Netherlands), with a step at $2\theta = 0.02^\circ$, scanning time of 2 s and Cu-Kα-radiation generated at 40 kV and 30 mA.

2.4.5. Fourier transform attenuated total reflectance infrared spectroscopy (FTIR-ATR)

The chemical structure of the samples before and after soaking in SBF was assessed by FTIR-ATR measurements using a Perkin–Elmer Spectrum Spotlight 200 FTIR Microscope System with the attenuated total reflection accessory. The spectra were acquired at room temperature in the 2000−400 cm^{-1} range by averaging 128 scans at a resolution of 4 cm^{-1}.

2.4.6. Inductively coupled plasma atomic emission spectrometry (ICP)

Inductively coupled plasma atomic emission spectrometry (ICP; JY 2000, Horiba Jobin Yvon) was used to measure elements concentration in SBF, before and after soaking the membranes.

2.4.7. Water contact angle (CA) measurements

The surface wettability of the samples was assessed by water contact angle measurements. These measurements were carried out by the sessile drop method using a contact angle meter (model OCA 15+) with a high-performance image processing system from DataPhysics Instruments (Filderstadt, Germany). A drop (3 μL) of water was added by a motor driven syringe at room temperature. Two different samples of each material were used and at least three measurements were carried out for each sample.

2.5. Dynamic mechanical analysis (DMA)

All viscoelastic measurements were performed using a TRITEC2000B DMA from Triton Technology (UK), equipped with the tensile mode. The measurements were carried out at 37 °C. The membrane samples were cut at about 4 mm width (measured accurately for each sample). CTS, CTS/μBG and CTS/nBG samples were always analyzed immersed in a liquid bath placed in a Teflon® reservoir. Two different experiments were performed: one was in real-time and the other one was offline. In the online experiments (data points collected every 1 s), two different solutions were used: PBS and SBF solutions. In the online measurements with SBF, the membranes were previously immersed in SBF up to equilibration and then the measurements were performed always keeping the membrane inside the apparatus. The motivation was to observe in real time the changes in the viscoelastic properties of the materials in a solution that induces mineralization. The other online experiment was performed with the membranes previously immersed in phosphate buffer saline (PBS) solution. PBS solution was chosen to see the viscoelastic behavior of the samples in a solution that does not induce the formation of an apatite layer.

The offline experiments were performed by measuring the sample in the DMA after being immersed in SBF for different periods. The procedure below was used for both online and offline experiments. The geometry of the samples was then measured and the samples were clamped in the DMA apparatus (the distance between the clamps was 10 mm) and immersed in the liquid bath. After equilibration at 37 °C, the DMA spectra were obtained during a frequency scan between 0.1 and 10 Hz. The experiments were performed under constant strain amplitude (30 μm) and at a strain of 2%. A static pre-load of 1 N was applied during the tests to keep the sample tight. Three specimens were tested for each condition.

3. Results and discussion

3.1. *Physical characterization of materials*

3.1.1. *Morphological characterization: TEM and SEM*

In this study, two different types of bioactive glass particles (micro, μBG, and nano, nBG) were used in the preparation of the composites (see Fig. 1). As show in Fig. 1, the nBG particles had a spherical somewhat interconnected appearance with particle size in the range 30–50 nm. Conversely, the μBG particles possess an irregular shape with particle size around 5 μm.

3.1.2. *Bioactivity tests*

3.1.2.1. SEM and EDS. The membranes were immersed in SBF for different time periods: 1 day, 5 days and 7 days. Fig. 1 shows representative SEM images and EDS spectra of the materials, which characterize the evolution of the apatite precipitation during the *in vitro* bioactivity tests. Both CTS/μBG and CTS/nBG composite membranes present an increase in the intensity of both calcium (Ca) and phosphorous (P) peaks with increasing soaking time in SBF. After only 1 day in SBF, an increase in the quantity of Ca and P is detected. After 7 days of immersion, strong peaks ascribed to Ca and P are observed indicating apatite-forming ability in SBF (Fig. 1). In the case of CTS membranes, no changes are observed by EDS, even after 7 days in SBF (Fig. 1), consistent with no apatite

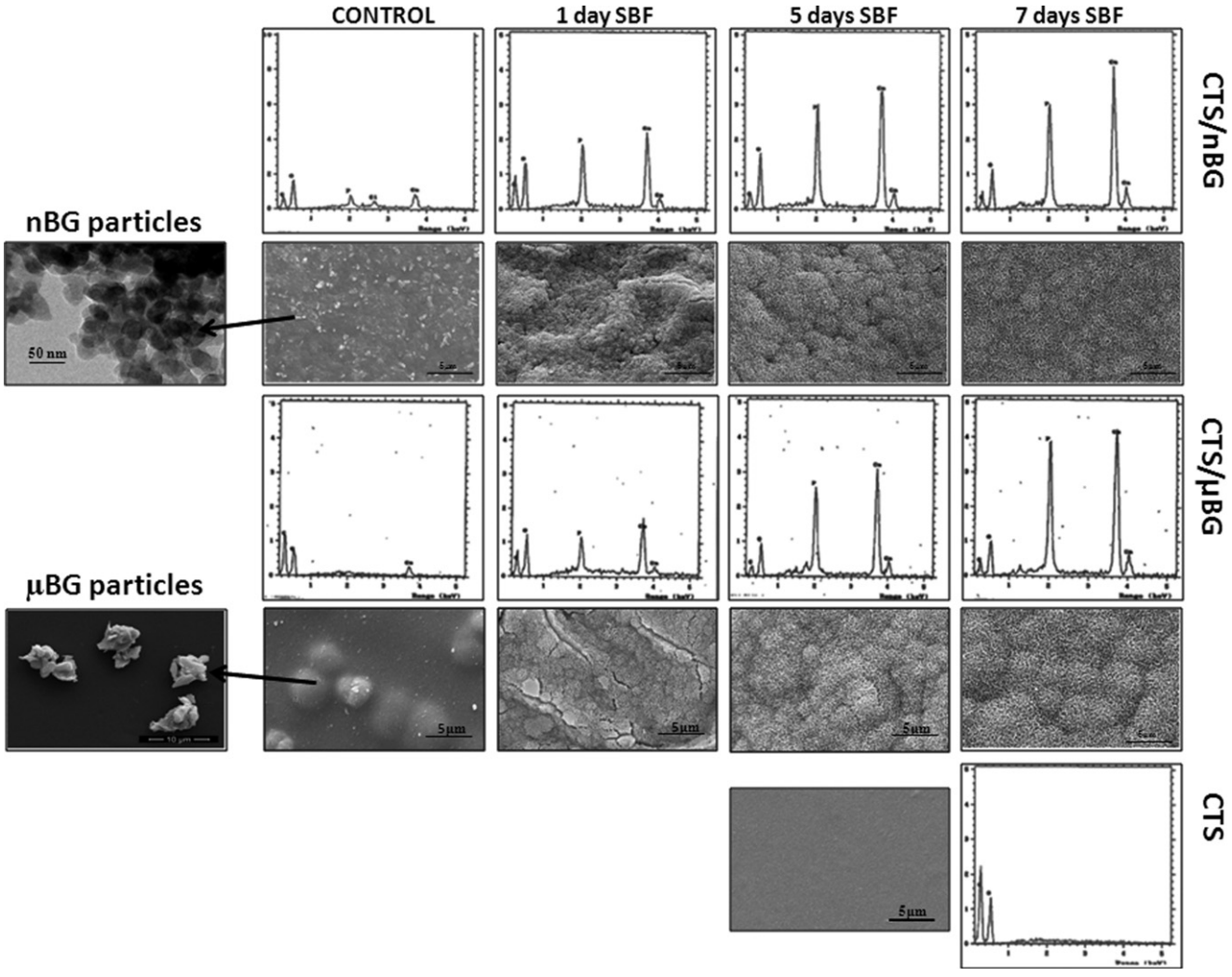

Fig. 1 – TEM image of the nBG particles and SEM image of the μBG particles prior to composite preparation. EDS spectra and SEM photographs of the surface of the CTS/nBG, CTS/μBG and CTS membranes after being soaked in SBF for different periods: 0 day (control), 1 day, 5 days and 7 days.

formation (lack of bioactivity). SEM images of the surface of the membranes before and after *in vitro* bioactivity tests are also presented in Fig. 1. CTS membranes exhibit a smooth surface. Conversely, the surface of both CTS/BG composite membranes show asperities corresponding to the presence of partially exposed BG particles which are homogeneously distributed in the entire surface. Comparing the morphology of the CTS/nBG and CTS/μBG membranes, a finer and rougher topography is observed in the case of the CTS/nBG membrane, this is a consequence of the smaller size of the inorganic particles in those membranes that should contribute to a more rapid formation of an apatite layer in agreement with previous results (Misra et al., 2008). Even after soaking in SBF for just 1 day, the composite samples could induce the precipitation of apatite (Fig. 1) with a thickness of $\sim 1.2 \pm 0.2$ μm and $\sim 0.8 \pm 0.2$ μm for the CTS/nBG and CTS/μBG samples, respectively. After 5 days of immersion in SBF the composite membrane was completely covered by a denser apatite layer, which increased in density after 7 days of soaking (Fig. 1). The typical cauliflower morphology of apatite crystals (Vallet-Regi, 2001) formed on bioactive surfaces after immersion in SBF is verified, which results from the assembling of nanometric-size needle-like crystals. The pure CTS membrane did not induce any apatite precipitation after immersion in SBF for 7 days (Fig. 1).

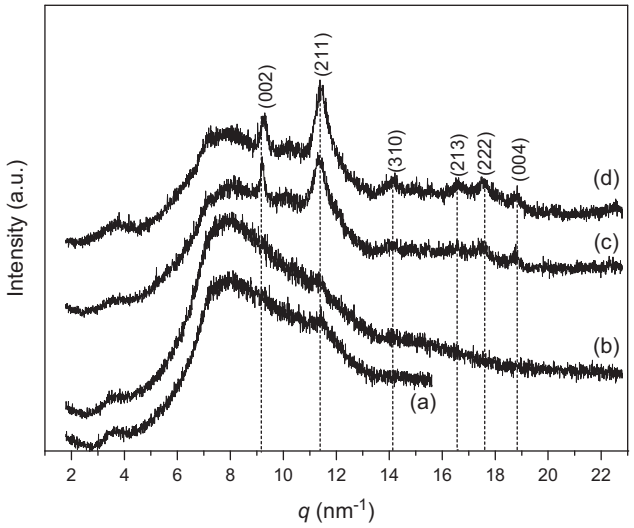

Fig. 2 – XRD patterns of the surface of the composite membranes before (CTS/μBG (a) and CTS/nBG (b)) and after being immersed for 7 days in SBF (CTS/μBG (c) and CTS/nBG (d)).

3.1.2.2. *TF-XRD*. The nature of the apatite layer formed *in vitro* was further characterized by XRD (Fig. 2). The XRD pattern of both CTS/BG control samples consisted of two major, broad crystalline Bragg peaks at around $q = 3.55$ and 7.10 nm^{-1} (Fig. 2a and b, respectively), that are ascribed to CTS (Teng et al., 2008). After 7 days of immersion in SBF, new broad peaks emerge in the patterns of both membranes, indicating that the layer formed is composed of nanocrystalline precipitates, possibly of similar dimensions to the ones found in bone. The reflections at $q = 9.19$ and 11.42 nm^{-1}, corresponding to diffraction planes (002) and (211), respectively, are characteristic of apatite, whereas those at 14.09, 16.49 and 19.38 nm^{-1} are associated with the diffraction planes (310), (213) and (004) of hydroxyapatite (ASTM JCPDS 9-432) (Leonor et al., 2008; Zainuddin et al., 2006).

3.1.2.3. *FTIR-ATR*. To get further insight into the apatite layer the FTIR spectra were examined. The FTIR spectrum of CTS displays a series of typical bands at: 3400 cm^{-1} (OH and NH stretching modes); 2913 and 2859 cm^{-1} (CH stretching modes) (Fig. 3(A)) and at 1655 and 1589 cm^{-1} (amide I and amide II modes, respectively); 1380 and 1319 cm^{-1} (C–CH_3 deformation mode) (Fig. 3(B)) (Wan et al., 2006). Although the spectra of both CTS/BG composite membranes contain the main characteristic bands of CTS, some additional bands emerge confirming the presence of BG particles. Such bands are located at 1020 cm^{-1} (Si–O–Si and P=O bands), 1000 cm^{-1} (Si–O NBO) and 758 cm^{-1} and 540–470 cm^{-1} (Si–O–Si) (Fig. 3(B)) (Cerruti et al., 2005; Marelli et al., 2010). After 7 days of

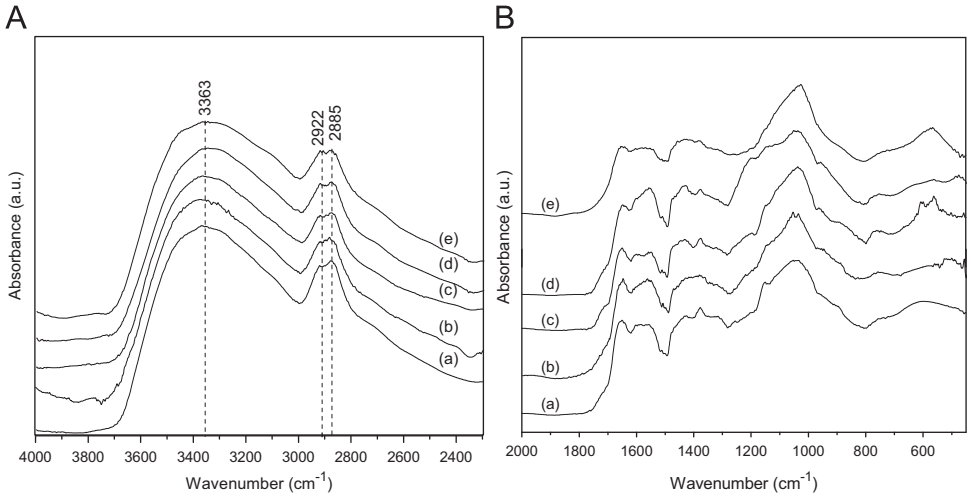

Fig. 3 – FTIR spectra of the surface of the membranes in the 4000–2300 cm^{-1} (A) and 2000–450 cm^{-1} (B) spectral intervals: CTS (a); CTS/μBG (b) and CTS/nBG (d) before being immersed for 7 days in SBF and CTS/μBG (c) and CTS/nBG (e) after being immersed for 7 days in SBF.

soaking in SBF, the FTIR spectra of both CTS/BG composite membranes exhibit characteristic phosphate and carbonate bands which provide evidence of the formation of an apatite layer. The absorption bands of the phosphate (PO_4^{3-}) groups are found between 1200–1030 cm^{-1} (asymmetric P–O stretching mode, υ_3), 962 cm^{-1} (P–O symmetric stretching mode, υ_1) and at 604 and 567 cm^{-1} (O–P–O bending mode, υ_4) (Fig. 3(B)) (Pleshko et al., 1991; Slosarczyk et al., 1997; van der Houwen et al., 2003). The absorption bands corresponding to the carbonate (CO_3^{2-}) groups are detected at 878 cm^{-1} (out-of-plane bending mode, υ_2), and 1650–1300 cm^{-1} (asymmetric stretching mode, υ_3, broad) (Fig. 3(B)) (Fleet, 2009). The broad, non-resolved envelope at 3700–330 cm^{-1} is due to the stretching mode of the OH groups (Fig. 3(A)). Comparing the spectra between the CTS/BG composite membranes, it is observed that the peaks of the CTS/nBG appear to be more narrowed than those of CTS/μBG. Taken all this information together, the results confirm the formation of an apatite layer on composite membranes which is similar to the major mineral component of vertebrate bone tissue.

3.1.2.4. ICP. ICP experiments allowed to determine the evolution of the concentration of ions in the SBF solution, namely Ca and P. Fig. 4 shows ICP results on SBF solutions after different immersion times. In the case of the solutions from the CTS membranes the concentrations of both Ca and P remain relatively constant, indicating again that this material does not have apatite-forming ability by itself. From the SBF extracts of both CTS/BG samples, a gradually decrease in Ca and P concentration was observed over the period of 7 days. The decrease in both Ca and P concentrations can be attributed to the consumption of these ions for the formation of the apatite layer. From literature (Peitl et al., 2001; Zeitler and Cormack, 2006), it is well known that an apatite layer is formed when bioactive glasses are placed in contact with the aqueous component of physiologic fluids and this process can be summarized in five stages (Peitl et al., 2001; Zeitler and Cormack, 2006). In the present case, when

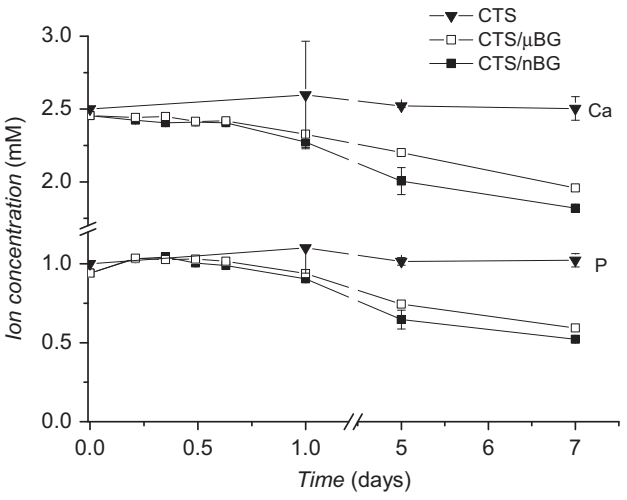

Fig. 4 – Change in Ca and P concentrations of SBF after the CTS, CTS/μBG and CTS/nBG membranes were immersed in SBF for different time periods up to 7 days, measured by ICP analysis.

the CTS/BG membranes are soaked in SBF, the Ca or sodium (Na) ions in the BG are released into the SBF solution (stage I), the soluble silica is loosen in the form of $Si(OH)_4$ to the solution as a result of the breakage of Si–O–Si bonds to form silanol groups (Si–OH) which induce apatite nucleation (stages II and III), as it is evident in Fig. 4 for the first time-points (before 1 day). Once apatite nuclei are formed, they can grow yielding a uniform layer by consuming the Ca and P ions from SBF (stages IV and V), as demonstrated by ICP experiments after 1 day. Thus, the induction period necessary for the Ca–P nucleation on the surface of the CTS/BG membranes is less than 24 h in SBF as a slight decrease in Ca and P concentration was observed even after 1 day. It is worth mentioning that a faster release of both Ca and P is observed in the case of CTS/nBG composite membranes indicating an enhanced bioactivity with respect to the CTS/μBG membranes.

In order to have more information about the apatite layer formed on the CTS/nBG membranes, SEM+EDS elemental mapping data was performed and results are presented in Fig. 5. Fig. 5 reproduces SEM+EDS mapping of silicon (Si), Ca and P along the thickness of the CTS/nBG membranes before and after 7 days of immersion in SBF. Before immersion in SBF, a uniform distribution of the nBG particles in the volume of the membrane is observed. After 7 days in SBF, the data shows that the Si content decreases, whereas the concentrations of Ca and P increases. This trend supports the finding that an apatite layer has developed. This apatite layer is well connected to the membrane, which was assessed qualitatively by SEM.

3.1.2.5. CA measurements. Cell–biomaterial interactions are strongly dependent on the wettability of the biomaterial's surface since this property determines several biological events such as protein adsorption, cell attachment and cell proliferation (Alves et al., 2010b; Lim et al., 2008). Water CAs were measured on selected samples, before and after being immersed either in SBF or PBS, to evaluate the wettability of the membranes with micron and nano-sized BG inclusions (Table 1). In the previous work, it has been reported that the use of SBF induce the formation of an apatite layer and the use of PBS did not induce apatite layer formation (Caridade et al., 2012). The aim of using such solutions was to see the effects by using a solution that induces mineralization on the material and another one that do not possess any effect on the materials. It is well-known that both topographic features and chemistry influence the wettability properties of surfaces. Before immersion in the solutions, CTS membranes have a contact angle of 93°±4 evidencing a hydrophobic character. After 7 days of immersion in SBF and in PBS, the CAs are 90°±6 and 92°±5, respectively, indicating that CTS essentially maintain their hydrophobic character. CTS/μBG membranes have a CA of 75°±6 due to the presence of μBG, which is a hydrophilic material. However, an increase in the CA is observed (86°±7) after 7 days of immersion in PBS, indicating that the μBG particles are being dissolved from the membranes. CTS/nBG membranes possess a CA of 65°±6 due the presence of the nBG and, when immersed in PBS over a period of 7 days, they have a contact angle of 81°±15 also due to the dissolution of the nBG particles. After 7 days in SBF,

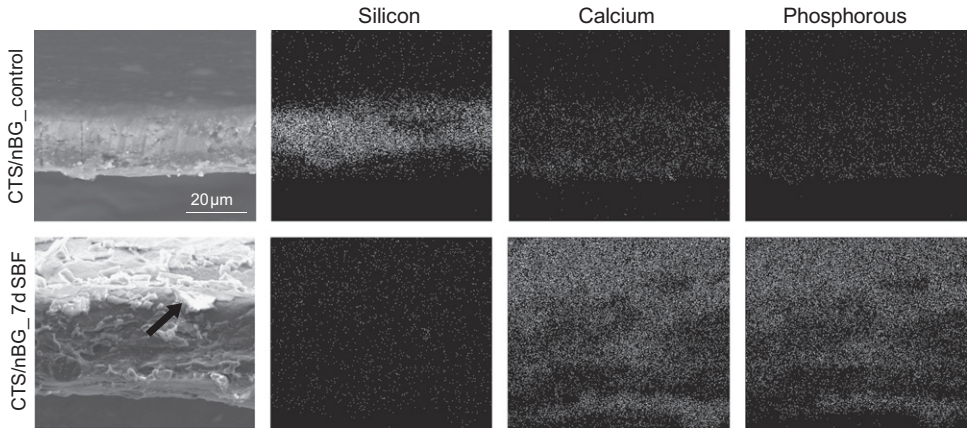

Fig. 5 – SEM+EDS elemental mapping of the CTS/nBG membrane before and after being soaked in SBF for 7 days evidencing the presence of silicon, calcium and phosphorous. The arrow points the apatite layer formed. The scale bar presented in the figure is the same for all images.

Table 1 – Water contact angle (θ) of CTS, CTS/μBG and CTS/nBG membranes before and after immersion in PBS and SBF: $**p<0.01$ and $***p<0.001$.

Sample/medium	$\theta(^\circ)$
CTS_ control	92.9° ± 3.6
CTS_ 7 days in PBS	91.6° ± 4.9
CTS_ 7 days in SBF	90.4° ± 6.3
CTS/μBG_ control	74.5° ± 6.5
CTS/nBG_ 7 days in PBS	86.4° ± 6.5
CTS/nBG_ control	65.0° ± 6.3
CTS/nBG_ 7 days in PBS	81.2° ± 14.6

[a]BG, biactive glass; [b]CTS; chitosan; [c]CTS/μBG, composite membranes made of chitosan and micron sized bioactive glass particles; [d]CTS/nBG, composite membranes made of chitosan and nano sized bioactive glass particles; [e]μBG, micron sized bioactive glass particles; [f]nBG, nano sized bioactive glass particles; [g]SBF, simulated body fluid solution; [h]E', storage modulus; [i]tan δ, loss factor; [j]PBS, phosphate buffer saline solution; [k]CTS/BG, composite membranes.

both CTS/BG composite samples became completely hydrophilic as the CA could not be measured. Such findings are correlated to the nature of the apatite layer formed on the surface, characterized by the assembly of hydrophilic calcium phosphate crystals forming a rough coating with a hierarchical organization at both the nano and micro levels (Fig. 1). Such combination of surface energy and topography leads to a surface exhibiting superhydrophilic properties. Analyzing all results together, the decrease in CA was more prominent for the CTS/nBG composites than for the CTS/μBG composites. This could be due to the fact that more of the nBG particles are exposed on the surface leading to increased interaction surface between the polymer and the glass particle inclusions facilitating water penetration.

3.2. *Dynamic mechanical analysis (DMA)*

3.2.1. *Offline monitoring of biomineralization*

DMA has been shown to be an adequate technique for characterizing the mechanical features of biomaterials (Mano, 2002) as one can use test conditions that closely simulate the physiological environment. It has been reported that biomaterials tested in buffered solutions at 37 °C exhibit a completely different viscoelastic behavior to the one observed in typical dry conditions (Ghosh et al., 2008; Mano and Reis, 2004). For example, previous studies on chitosan showed that upon immersion of the material in water a profound effect in its mechanical properties is verified in which E' shows a reduction in a factor of 50 during the wetting process (Mano, 2008). Silva et al. (2004) demonstrate that even in neutral pH aqueous media, where the amine groups are not protonated, chitosan membranes absorb up to about 150 wt% of water (Silva et al., 2004). Such absorption takes place in few minutes during which the glass transition of the biopolymer takes place. This behavior has been demonstrated by performing DMA studies on chitosan membranes immersed in mixtures of water/ethanol with different compositions where the strong decrease in the loss modulus of chitosan upon water uptake could be mainly a consequence of the glass transition event (Caridade et al., 2009). For that reason, performing mechanical tests on biomaterials with water uptake capability under physiological-like conditions is of major importance. In this study, offline DMA experiments were carried out to

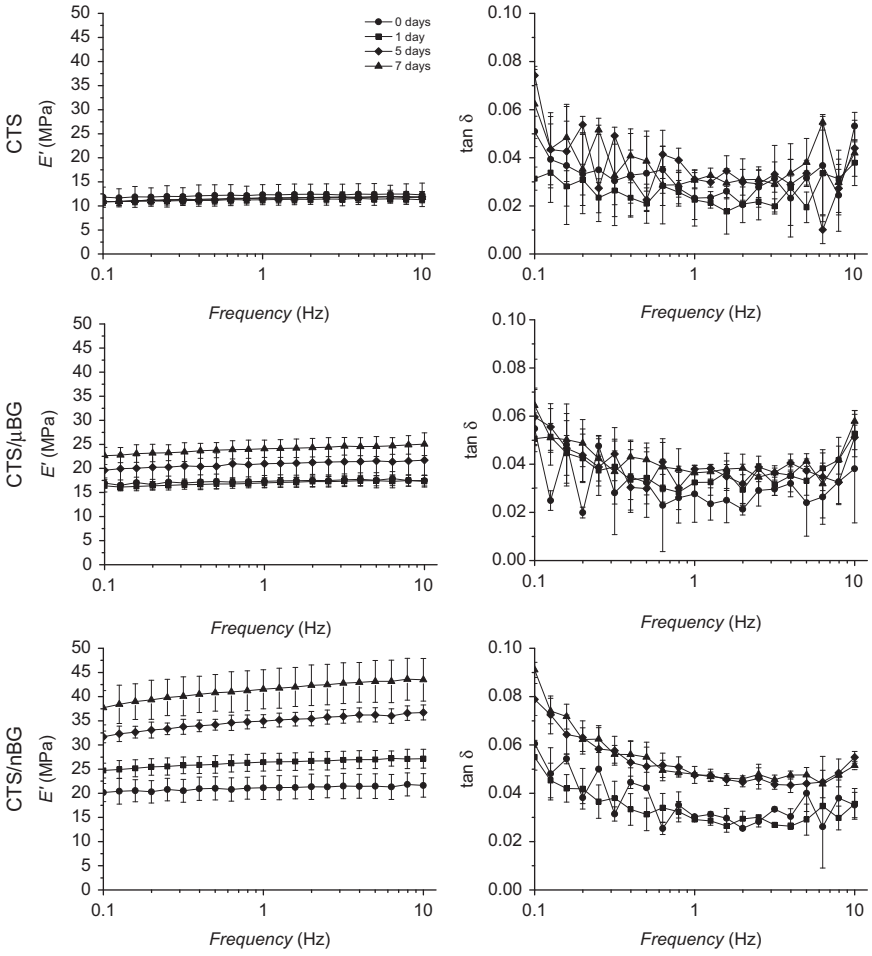

Fig. 6 – DMA scans of CTS, CTS/μBG and CTS/nBG membranes obtained under immersion in SBF at 37 °C after being previously immersed in SBF for different time periods: ●, 0 day; ■, 24 h; ♦, 5 days; ▲, 7 days.

monitor the variations of the viscoelastic properties of the samples upon immersion in SBF. Fig. 6 shows DMA results obtained by frequency scans on the samples that were previously soaked in SBF for different times. A small increase in E' with increasing frequency is verified for all samples. In the case of the CTS membranes, all scans are superimposed and the data are similar to those obtained in water immersion tests (Mano, 2008) indicating that the viscoelastic properties of CTS are independent of the immersion time in SBF. Oppositely, both CTS/BG composite membranes present a completely different behavior: E' increases with increasing soaking time. This stiffening effect induced by the immersion of the CTS/BG membranes in SBF should be a result of the development of an apatite layer over the surfaces of the samples. Before the static soaking stage in SBF the E' of both CTS/BG membranes is higher than the one of the pure CTS membrane, a result that can be explained by the reinforcing effect of the BG particles in the composite materials. Comparing the two composite membranes, CTS/nBG presents E' higher than the E' of CTS/μBG (20 MPa and 17 MPa, respectively). Misra et al. (2008) also reported that the addition of such kind of nanoparticles has a significant stiffening effect in biodegradable polymer matrices. This stiffening effect is even more pronounced with increasing soaking time in SBF after 7 days in SBF E' of CTS/nBG is about 37 MPa and E' of CTS/μBG is about 22 MPa. Compared with μBG particles, nBG particles have a larger surface area forming a tighter interface with the polymer matrix in the composite, thus a higher load transfer effect is expected leading to enhanced composite stiffness.

Fig. 6 also represents the variation of the tan δ along the frequency. The loss factor is the ratio of the amount of energy dissipated by viscous mechanisms relative to energy stored in the elastic component providing information about the damping properties of the material. For all formulations, tan δ tends to decrease with the increase in frequency indicating that the materials became less viscous and more elastic. Moreover, from Fig. 6, it was observed that the tan δ exhibited higher values for CTS/nBG than CTS and CTS/μBG membranes indicating that such materials possess higher capacity to dissipate energy. This could be the result of the larger area covered by the interface between the polymeric matrix and the particles for the former composite, that could contribute more for the dissipation of mechanical energy. In a general point of view, the tan δ values of the composite membranes do not exhibit significant variation with the previous immersion period in SBF. This means that the *in vitro* mineralization process of the biomaterial does not influence significantly its damping properties.

3.2.2. *Online monitoring of biomineralization*

In the present work, online DMA experiments have been also performed. The motivation for these experiments is that if the biomaterial possesses osteoconductive properties it should promote the deposition of hydroxyapatite on its surface and its mechanical properties will continuously change. DMA experiments were used to monitor the change in the viscoelastic properties of the samples immersed in both PBS and SBF during the first 24 h (see Fig. 7(A)). No changes in *E'* for the CTS membrane are observed with increasing immersion time, indicating that, as expected, during this period no mineralization, degradation or other processes that could change the mechanical behavior take place in the pure biopolymer membrane. The same behavior is observed for CTS membranes when immersed in PBS. On the other hand, when immersed in PBS, *E'* of both CTS/BG composite membranes present a continuous decrease. This loss of stiffness is ascribed to the fact that the BG particles are being dissolved from the membranes and the result is consistent with the information obtained by CA measurements. When immersed in SBF, a totally different evolution of *E'* is verified for both CTS/BG composites as in the case of PBS, the *E'* decreases continuously up to ca. 7 h (in the case of CTS/μBG) and up to ca. 4 h (for CTS/nBG) of immersion in SBF indicating that the BG particles are being dissolved from the membranes. After such periods of time *E'* stabilizes and starts to increase, with increasing immersion time in SBF. The increase in *E'* is more pronounced after 15 h for the CTS/μBG and after 8 h for the CTS/nBG, indicating that a hydroxyapatite layer is being formed. To reinforce this hypothesis, SEM observations were performed for short immersion time in SBF on the CTS/BG composite membranes. From SEM images shown in Fig. 7(B) it is observed that after 5 h no hydroxyapatite layer is formed on the CTS/nBG sample, which is consistent with the dissolution of the nanoparticles from the membrane, thus *E'* decreases. On the other hand, after 8 h of immersion in SBF, the CTS/nBG membrane presents some apatite formed on the surface that is associated to the increase in *E'* of the CTS/nBG composite membrane. For the CTS/μBG membranes the presence of a hydroxyapatite layer could be detected after a period of 15 h (Fig. 7(B)). DMA experiments also demonstrate being a non-destructive technique allowing the monitoring of the apatite layer formation. In fact, bioactivity tests were made separately, in static conditions, and the morphology of the apatite layer formed observed by SEM was the same as the ones obtained after the samples being tested in DMA (data not shown). Interestingly, such results demonstrate that a faster kinetic of hydroxyapatite formation is obtained by using nanoparticles. Thus the use of nanoparticles proves to have the following advantages: (i) using nanosized particles in the CTS matrix induces a tighter interface leading to an effective increase of the Young' s modulus; (ii) the higher specific surface area of the nanoparticles allows a faster release of ions, namely Ca and P, enhancing the

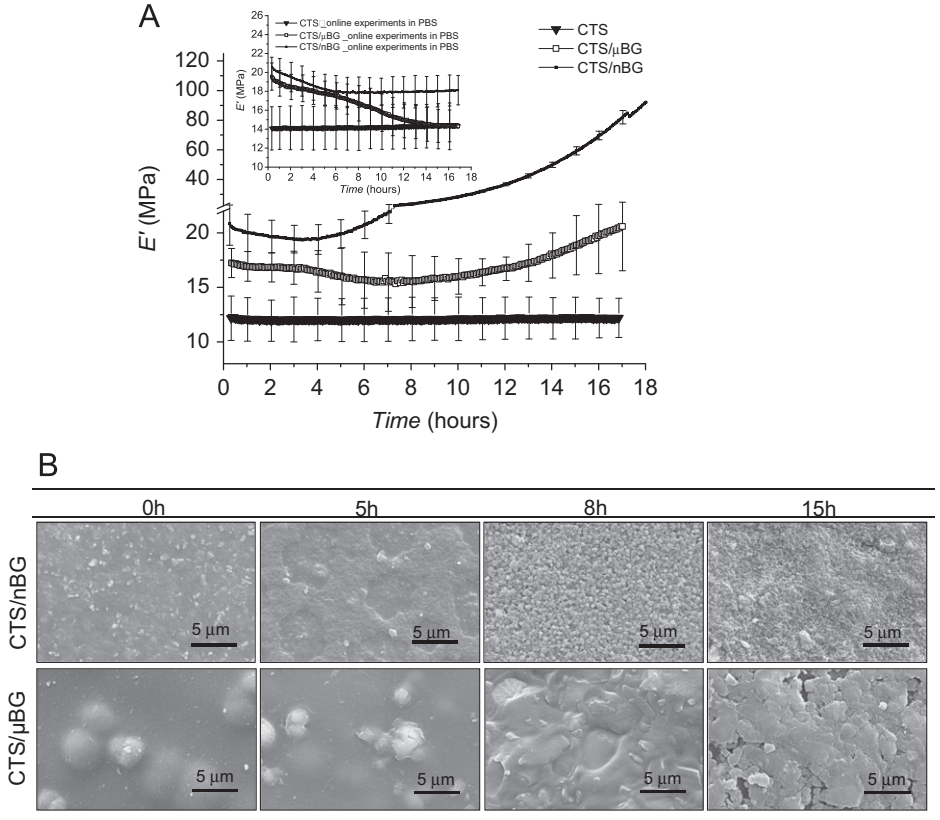

Fig. 7 – (A) Online DMA measurements at 1 Hz on the CTS and both CTS/BG membranes while immersed in SBF for the first 24 h. The inset represents the same online DMA experiments on CTS/nBG membranes while immersed in PBS for the first 24 h. (B) SEM images on the surface of both the CTS/BG composites membranes taken after short immersion times in SBF (0 h, 5 h, 8 h, and 15 h).

bioactivity formation of a hydroxyapatite surface layer of such composites; and (iii) the use of nBG in the CTS matrix mimics more closely the structure of natural bone than if micrometer-sized particles are used. Similar membrane composites combining chitosan and silica-based bioactive nanoparticles, prepared by sol–gel, were also found to elicit favorable biological activity *in vitro* (Luz and Mano, 2012; Mota et al., 2012), which enhances the potential applicability of such kind of systems for a series of biomedical applications, including in the orthopedic and maxillo-facial fields.

4. Conclusions

CTS, CTS/μBG and CTS/nBG membranes were prepared by solvent casting at room temperature. Both CTS/BG composite membranes presented improved mechanical properties and excellent hydroxyapatite forming ability compared to pure CTS membrane. This study has highlighted the advantages of using nano-sized bioactive particles over conventional (micron-sized) bioactive glasses, which result from the large surface area of the nBG; CTS/nBG composite membranes presented enhanced performance in the mechanical properties and enhanced bioactivity. For the first time in this class of composites, the biomineralization process was followed, in real time, using *in situ* DMA where a faster mineralization kinetic was observed for the CTS/nBG composite: a period of 8 h was sufficient to induce an increase of stiffness due to enhanced deposition of hydroxyapatite as compared with a period of 15 h required for apatite formation in the CTS/μBG membranes.

Acknowledgments

This work was financially supported by Foundation for Science and Technology (FCT) by the projects PTDC/QUI/69263/2006, PTDC/CTM-BPC/112774/2009 and, through the scholarship SFRH/BD/64601/2009 granted to Sofia G. Caridade. The authors acknowledge Dr D. Mohn and Prof. W. Stark (ETH Zurich) for providing the nBG particles used.

REFERENCES

Alves, N.M., Leonor, I.B., Azevedo, H.S., Reis, R.L., Mano, J.F., 2010a. Designing biomaterials based on biomineralization of bone. Journal of Materials Chemistry 20 (15), 2911–2921.

Alves, N.M., Pashkuleva, I., Reis, R.L., Mano, J.F., 2010b. Controlling cell behavior through the design of polymer surfaces. Small 6 (20), 2208–2220.

Boccaccini, A.R., Erol, M., Stark, W.J., Mohn, D., Hong, Z., Mano, J.F., 2010. Polymer/bioactive glass nanocomposites for biomedical applications: A review. Composites Science and Technology 70 (13), 1764–1776.

Brunner, T.J., Grass, R.N., Stark, W.J., 2006. Glass and bioglass nanopowders by flame synthesis. Chemical Communications 13, 1384–1386.

Caridade, S.G., da Silva, R.M.P., Reis, R.L., Mano, J.F., 2009. Effect of solvent-dependent viscoelastic properties of chitosan membranes on the permeation of 2-phenylethanol. Carbohydrate Polymers 75 (4), 651–659.

Caridade, S.G., Merino, E.G., Alves, N.M., Mano, J.F., 2012. Bioactivity and viscoelastic characterization of chitosan/bioglass® composite membranes. Macromolecular Bioscience 12 (8), 1106–1113.

Cerruti, M., Greenspan, D., Powers, K., 2005. Effect of pH and ionic strength on the reactivity of Bioglass (R) 45S5. Biomaterials 26 (14), 1665–1674.

da Silva, R.M.P., Mano, J.F., Reis, R.L., 2008. Straightforward determination of the degree of *N*-acetylation of chitosan by means of first-derivative UV spectrophotometry. Macromolecular Chemistry and Physics 209 (14), 1463–1472.

Ebenstein, D.M., Pruitt, L.A., 2004. Nanoindentation of soft hydrated materials for application to vascular tissues. Journal of Biomedical Materials Research Part A 69A (2), 222–232.

Ebenstein, D.M., Pruitt, L.A., 2006. Nanoindentation of biological materials. Nano Today 1 (3), 26–33.

Eliaz, N., Kopelovitch, W., Burstein, L., Kobayashi, E., Hanawa, T., 2009. Electrochemical processes of nucleation and growth of calcium phosphate on titanium supported by real-time quartz crystal microbalance measurements and X-ray photoelectron spectroscopy analysis. Journal of Biomedical Materials Research Part A 89A (1), 270–280.

Fleet, M.E., 2009. Infrared spectra of carbonate apatites: υ (2)-region bands. Biomaterials 30 (8), 1473–1481.

Franke, O., Durst, K., Maier, V., Goken, M., Birkhoiz, T., Schneider, H., Hennig, F., Gelse, K., 2007. Mechanical properties of hyaline and repair cartilage studied by nanoindentation. Acta Biomaterialia 3 (6), 873–881.

Franke, O., Goken, M., Meyers, M.A., Durst, K., Hodge, A.M., 2011. Dynamic nanoindentation of articular porcine cartilage. Materials Science and Engineering **C**: Materials for Biological Applications 31 (4), 789–795.

Ghosh, S., Gutierrez, V., Fernandez, C., Rodriguez-Perez, M.A., Viana, J.C., Reis, R.L., Mano, J.F., 2008. Dynamic mechanical behavior of starch-based scaffolds in dry and physiologically simulated conditions: Effect of porosity and pore size. Acta Biomaterialia 4 (4), 950–959.

Gloria, A., De Santis, R., Ambrosio, L., 2010. Polymer-based composite scaffolds for tissue engineering. Journal of Applied Biomaterials and Biomaterials 8 (2), 57–67.

Hench, L.L., 1998. Bioceramics. Journal of the American Ceramic Society 81 (7), 1705–1728.

Hong, Z.K., Zhang, P.B., He, C.L., Qiu, X.Y., Liu, A.X., Chen, L., Chen, X.S., Jing, X.B., 2005. Nano-composite of poly(L-lactide) and surface grafted hydroxyapatite: mechanical properties and biocompatibility. Biomaterials 26 (32), 6296–6304.

Juhasz, J.A., Best, S.M., Brooks, R., Kawashita, M., Miyata, N., Kokubo, T., Nakamura, T., Bonfield, W., 2004. Mechanical properties of glass-ceramic A-W-polyethylene composites: effect of filler content and particle size. Biomaterials 25 (6), 949–955.

Kay, S., Thapa, A., Haberstroh, K.M., Webster, T.J., 2002. Nanostructured polymer/nanophase ceramic composites enhance osteoblast and chondrocyte adhesion. Tissue Engineering 8 (5), 753–761.

Kim, H.W., Kim, H.E., Salih, V., 2005a. Stimulation of osteoblast responses to biomimetic nanocomposites of gelatin-hydroxyapatite for tissue engineering scaffolds. Biomaterials 26 (25), 5221–5230.

Kim, H.W., Song, J.H., Kim, H.E., 2005b. Nanofiber generation of gelatin-hydroxyapatite biomimetics for guided tissue regeneration. Advanced Functional Materials 15 (12), 1988–1994.

Kokubo, T., Takadama, H., 2006. How useful is SBF in predicting in vivo bone bioactivity? Biomaterials 27 (15), 2907–2915.

Leonor, I.B., Baran, E.T., Kawashita, M., Reis, R.L., Kokubo, T., Nakamura, T., 2008. Growth of a bonelike apatite on chitosan

microparticles after a calcium silicate treatment. Acta Biomaterialia 4 (5), 1349–1359.
Leonor, I.B., Ito, A., Onuma, K., Kanzaki, N., Reis, R.L., 2003. In vitro bioactivity of starch thermoplastic/hydroxyapatite composite biomaterials: an *in situ* study using atomic force microscopy. Biomaterials 24 (4), 579–585.
Lim, J.Y., Shaughnessy, M.C., Zhou, Z.Y., Noh, H., Vogler, E.A., Donahue, H.J., 2008. Surface energy effects on osteoblast spatial growth and mineralization. Biomaterials 29 (12), 1776–1784.
Loher, S., Reboul, V., Brunner, T.J., Simonet, M., Dora, C., Neuenschwander, P., Stark, W.J., 2006. Improved degradation and bioactivity of amorphous aerosol derived tricalcium phosphate nanoparticles in poly (lactide-co-glycolide). Nanotechnology 17 (8), 2054–2061.
Luz, G.M., Mano, J.F., 2010. Mineralized structures in nature: Examples and inspirations for the design of new composite materials and biomaterials. Composites Science and Technology 70 (13), 1777–1788.
Luz, G.M., Mano, J.F., 2012. Chitosan/bioactive glass nanoparticles composites for biomedical applications. Biomedical materials 7 (5), 054104.
Madler, L., Kammler, H.K., Mueller, R., Pratsinis, S.E., 2002. Controlled synthesis of nanostructured particles by flame spray pyrolysis. Journal of Aerosol Science 33 (2), 369–389.
Mano, J.F., 2008. Viscoelastic properties of chitosan with different hydration degrees as studied by dynamic mechanical analysis. Macromolecular Bioscience 8 (1), 69–76.
Mano, J.F., Reis, R.L., 2004. Viscoelastic monitoring of starch-based biomaterials in simulated physiological conditions. Materials Science and Engineering A-Structural Materials Properties Microstructure and Processing 370 (1–2), 321–325.
Mano, J.F., Reis, R.L., Cunha, A.M., 2002. Dynamic mechanical analysis in polymers for medical applications. In: Reis, R.L., Cohn, D. (Eds.), Polymer Based Systems on Tissue Engineering, Replacement and Regeneration. Kluwer Academic Publishers, Netherlands, pp. 139–164.
Marelli, B., Ghezzi, C.E., Barralet, J.E., Boccaccini, A.R., Nazhat, S.N., 2010. Three-dimensional mineralization of dense nanofibrillar collagen – bioglass hybrid scaffolds. Biomacromolecules 11 (6), 1470–1479.
Misra, S.K., Mohn, D., Brunner, T.J., Stark, W.J., Philip, S.E., Roy, I., Salih, V., Knowles, J.C., Boccaccini, A.R., 2008. Comparison of nanoscale and microscale bioactive glass on the properties of P(3HB)/Bioglass® composites. Biomaterials 29 (12), 1750–1761.
Mota, J., Yu, N., Caridade, S.G., Luz, G.M., Gomes, M.E., Reis, R.L., Jansen, J.A., Walboomers, X.F., Mano, J.F., 2012. Chitosan/bioactive glass nanoparticle composite membranes for periodontal regeneration. Acta Biomaterialia 8 (11), 4173–4180.
Nayar, V.T., Weiland, J.D., Nelson, C.S., Hodge, A.M., 2012. Elastic and viscoelastic characterization of agar. Journal of the Mechanical Behavior of Biomedical Materials 7, 60–68.
Oliveira, A.L., Mano, J.F., Reis, R.L., 2003. Nature-inspired calcium phosphate coatings: present status and novel advances in the science of mimicry 7 (4–5), 309–318. Current Opinion in Solid State & Materials Science 7 (4–5), 309–318.
Palin, E., Liu, H.N., Webster, T.J., 2005. Mimicking the nano-features of bone increases bone-forming cell adhesion and proliferation. Nanotechnology 16 (9), 1828–1835.
Peitl, O., Zanotto, E.D., Hench, L.L., 2001. Highly bioactive P_2O_5–Na_2O–CaO–SiO_2 glass-ceramics. Journal of Non-Crystalline Solids 292 (1–3), 115–126.
Pleshko, N., Boskey, A., Mendelsohn, R., 1991. Novel infrared spectroscopic method for the determination of crystallinity of hydroxyapatite minerals. Biophysical Journal 60 (4), 786–793.
Rezwan, K., Chen, Q.Z., Blaker, J.J., Boccaccini, A.R., 2006. Biodegradable and bioactive porous polymer/inorganic composite scaffolds for bone tissue engineering. Biomaterials 27 (18), 3413–3431.
Silva, R.M., Silva, G.A., Coutinho, O.P., Mano, J.F., Reis, R.L., 2004. Preparation and characterisation in simulated body conditions of glutaraldehyde crosslinked chitosan membranes. The Journal of Materials Science: Materials in Medicine 15 (10), 1105–1112.
Slosarczyk, A., Paluszkiewicz, C., Gawlicki, M., Paszkiewicz, Z., 1997. The FTIR spectroscopy and QXRD studies of calcium phosphate based materials produced from the powder precursors with different Ca/P ratios. Ceramics International 23 (4), 297–304.
Strange, D.G.T., Oyen, M.L., 2012. Composite hydrogels for nucleus pulposus tissue engineering. Journal of the Mechanical Behavior of Biomedical Materials 11, 16–26.
Swetha, M., Sahithi, K., Moorthi, A., Srinivasan, N., Ramasamy, K., Selvamurugan, N., 2010. Biocomposites containing natural polymers and hydroxyapatite for bone tissue engineering. International Journal of Biological Macromolecules 47 (1), 1–4.
Teng, S.H., Lee, E.J., Wang, P., Shin, D.S., Kim, H.E., 2008. Three-layered membranes of collagen/hydroxyapatite and chitosan for guided bone regeneration. Journal of Biomedical Materials Research Part B-Applied Biomaterials 87B (1), 132–138.
Terbojevich, M., Cosani, A., Muzzarelli, R.A.A., 1996. Molecular parameters of chitosans depolymerized with the aid of papain. Carbohydrate Polymers 29 (1), 63–68.
Vallet-Regi, M., 2001. Ceramics for medical applications. Journal of the Chemical Society, Dalton 2, 97–108.
van der Houwen, J.A.M., Cressey, G., Cressey, B.A., Valsami-Jones, E., 2003. The effect of organic ligands on the crystallinity of calcium phosphate. Journal of Crystal Growth 249 (3-4), 572–583.
Vollenweider, M., Brunner, T.J., Knecht, S., Grass, R.N., Zehnder, M., Imfeld, T., Stark, W.J., 2007. Remineralization of human dentin using ultrafine bioactive glass particles. Acta Biomaterialia 3 (6), 936–943.
Wan, Y., Wu, H., Yu, A.X., Wen, D.J., 2006. Biodegradable polylactide/chitosan blend membranes. Biomacromolecules 7 (4), 1362–1372.
Webster, T.J., Siegel, R.W., Bizios, R., 1999. Osteoblast adhesion on nanophase ceramics. Biomaterials 20 (13), 1221–1227.
Wheeler, D.L., Stokes, K.E., Hoellrich, R.G., Chamberland, D.L., McLoughlin, S.W., 1998. Effect of bioactive glass particle size on osseous regeneration of cancellous defects. Journal of Biomedical Materials Research 41 (4), 527–533.
Zainuddin, Hill, D.J.T., Chirila, T.V., Whittaker, A.K., Kemp, A., 2006. Experimental calcification of HEMA-based hydrogels in the presence of albumin and a comparison to the in vivo calcification. Biomacromolecules 7 (6), 1758–1765.
Zeitler, T.R., Cormack, A.N., 2006. Interaction of water with bioactive glass surfaces. Journal of Crystal Growth 294 (1), 96–102.